Table 1 Pressure's value on the circular obstacle

Elements	1	2	3	4	5
Exact	0.987	0.891	0.707	0.454	0.156
This meth.	0.917	0.903	0.717	0.463	0.170
Elements	6	7	8	9	10
Exact	−0.156	−0.454	−0.707	−0.891	−0.987
This meth.	−0.170	−0.463	−0.717	−0.903	−0.917

we deduce

$$2\pi a_{ij} = -r(y_1 + y_2 - 2y_1)i_0 - r(y_2 - y_i)i_1 \tag{24}$$

where

$$i_0 = \frac{1}{d} \text{ arc } tg \frac{2dr^2}{b^2 + d^2 - r^4}$$

$$i_1 = \frac{1}{2r^2} \ell_n \frac{r^2 + 2b + c}{r^2 - 2b + c} - \frac{b}{dr^2} \text{arc } tg \frac{2dr^2}{b^2 + d^2 - r^4} \tag{25}$$

Since $x_1 + x_2 = 2x_j$, $y_1 + y_2 = 2y_j$ we deduce $a_{ii} = 0$.

V. Numerical Results

As a test we use the circular obstacle in an incompressible fluid. In this case the exact solution is known. Table 1 gives the exact values and the values calculated with this method for the pressure on the quarter of the circle starting with the upper point and proceeding clockwise. The pressure distribution is symmetric. The results are very good. This is also confirmed in the case of the elliptic obstable.

In Fig. 1 we gave C_p calculated with the formula

$$C_p = \frac{P_1 - p_\infty}{(1/2)\rho_\infty U_\infty^2} = \frac{2p}{\beta}$$

for an airfoil of aerodynamic interest in incompressible flow at indicated incidences. The data in the catalogues of airfoil sections also confirm these results.

References

[1]Karamcheti, K., *Principles of Ideal-Fluid Aerodynamics*, John Wiley, New York, 1966, Ch. 17.

[2]Hess J. L., and Smith, A. M. O., "Calculation of Nonlifting Potential Flow about Arbitrary Three-dimensional Bodies," *Journal of Ship Research*, Sept. 1964, pp. 22-44.

[3]Brebbia, C. A., Telles, J. C. F., and Wrobel, L. C., "Boundary Element Techniques," *Theory and Application in Engineering*, Springer-Verlag, Berlin, 1984, Ch. 2.

[4]Dragos, L., "Boundary Element Methods (BEM) in the Theory of Thin Airfoils," *Rev. Roum. Math. Pures et Appl.*, Vol. 34, No. 6, 1989, p. 523.

[5]Dragos, L., "Method of Fundamental Solutions in Plane Steady Linear Aerodynamics," *Acta Mechanica*, Vol. 47, No. 3-4, 1983, p. 277.

[6]Stakgold, I., *Boundary Value Problems of Mathematical Physics*, Vol. 2, Macmillan, New York, 1968, p. 6.

Analytic Relation for the Holstein-Bohlen Pressure Gradient Parameter

Everett Jones*
University of Maryland, College Park, Maryland 20742

Introduction

THE classic integral boundary-layer method of Holstein and Bohlen is presented in many texts such as White.[1] The method, while unsatisfactory in some respects, still has academic interest. It was, of course, conceived in an era where hand calculations were necessary. Therefore, the fact that the expressions for the boundary-layer quantities of interest are expressed in terms of the pressure-gradient parameter, Λ for the von Karman-Pohlhausen method instead of the pressure gradient parameter K for the Holstein-Bohlen method, presents no significant difficulty. In order to avoid table look-up operations in computer codes, a function $\Lambda(K)$ would allow routine calculations for all quantities. The analysis reported here resulted in a relatively simple, accurate correlation for $\Lambda(K)$.

In a classic solution of the von Karman[2] momentum integral equation for incompressible flow,

$$\tau_w = \rho_e \frac{d(u_e^2\Theta)}{dx} + \rho_e u_e \delta^* \frac{du_e}{dx}$$

$$= \rho_e u_e^2 \frac{d\Theta}{dx} + (2\Theta + \delta^*)\rho_e u_e \frac{du_e}{dx} \tag{1}$$

Pohlhausen[3] assumed the fourth-order polynomial in Eq. (2) for the velocity profile.

$$\frac{u}{u_e} = \sum_{n=0}^{4} a_n(x)\xi^n \qquad \text{for } 0 \le \xi = \frac{y}{\delta(x)} \le 1$$

$$= 1 \qquad \text{for } \xi \ge 1 \tag{2}$$

This polynomial has five coefficients that are related to local conditions on the velocity profile. The minimum conditions are the no-slip boundary condition and the edge condition on velocity. Two conditions guaranteed the asymptotic behavior of the first two derivatives of the velocity at the boundary-layer edge and the last condition was the lowest-order compatibility condition. The resulting velocity profile is

$$\frac{u}{u_e} = 2\xi - 2\xi^3 + \xi^4 + \frac{\Lambda(x)}{6}(\xi - 3\xi^2 + 3\xi^3 - \xi^4)$$

$$\text{for } 0 \le \xi \le 1 \text{ with } \Lambda(x) = \frac{\delta^2}{\nu}\frac{du_e}{dx} \tag{3}$$

where Λ is the pressure-gradient parameter. Then, the displacement and momentum thicknesses are related to the boundary-layer thickness by

$$\delta^* = \text{the displacement thickness} = \int_0^\delta \left(1 - \frac{u}{u_e}\right) dy$$

$$= \frac{\delta}{10}\left(3 - \frac{\Lambda}{12}\right) \tag{4}$$

Received Jan. 22, 1990; revision received Feb. 16, 1990.

*Associate Professor. Member AIAA.

$$\Theta = \text{the momentum thickness} = \int_0^{\delta} \frac{u}{u_e}\left(1-\frac{u}{u_e}\right) dy$$

$$= \delta\left(\frac{37}{315} - \frac{\Lambda}{945} - \frac{\Lambda^2}{9072}\right) \tag{5}$$

and the wall shear stress is

$$\frac{\delta\tau_w}{\mu u_e} = 2 + \frac{\Lambda}{6} \tag{6}$$

Substitution of Eqs. (4-6) into Eq. (1) produces a differential equation requiring evaluation of the second derivative of edge velocity, $u_e(x)$, through the derivative of Θ.

Holstein and Bohlen[4] multiplied Eq. (1) by $\Theta/\mu u_e$ to obtain

$$\frac{\tau_w\Theta}{\mu u_e} = \frac{u_e}{\nu}\Theta\frac{d\Theta}{dx} + \left(2+\frac{\delta^*}{\Theta}\right)\frac{\Theta^2}{\nu}\frac{du_e}{dx}$$

$$= \frac{u_e}{2}\frac{d}{dx}\left(\frac{\Theta^2}{\nu}\right) + \left(2+\frac{\delta^*}{\Theta}\right)\frac{\Theta^2}{\nu}\frac{du_e}{dx} \tag{7}$$

The pressure-gradient parameter $K(x)$ suggested by this equation can be related to the pressure-gradient parameter of Pohlhausen by

$$K(x) = Z\frac{du_e}{dx} = \frac{\Theta^2}{\nu}\frac{du_e}{dx} = \left(\frac{\Theta}{\delta}\right)^2\Lambda$$

$$= \left(\frac{37}{315} - \frac{\Lambda}{945} - \frac{\Lambda^2}{9072}\right)^2\Lambda, \qquad Z = \frac{\Theta^2}{\nu} \tag{8}$$

Equation (8) can be regarded as an inverse relation for $\Lambda(K)$ such that δ^*/Θ and $\Theta\tau_w/\mu u_e$ in Eq. (7) can be regarded to be functions of K as follows:

$$\frac{\delta^*}{\Theta} = \frac{\left(\frac{3}{10} - \frac{\Lambda}{120}\right)}{\left(\frac{37}{315} - \frac{\Lambda}{945} - \frac{\Lambda^2}{9072}\right)^2} = f_1(K),$$

$$\frac{\Theta\tau_w}{\mu u_e} = \left(2+\frac{\Lambda}{6}\right)\left(\frac{37}{315} - \frac{\Lambda}{945} - \frac{\Lambda^2}{9072}\right) = f_2(K) \tag{9}$$

and Eq. (7) can be rewritten as

$$u_e\frac{dZ}{dx} = 2\{f_2(K) - K[2 + f_1(K)]\} = F_1(K)$$

$$\text{or} \qquad \frac{dZ}{dx} = \frac{F_1(K)}{u_e} \tag{10}$$

An analytic function for $\Lambda(K)$ requires solution of the fifth-order algebraic equation, Eq. (8), and such a function has not been derived. Instead, a table has traditionally been used with the analyst performing the table look-up operation to obtain the functions $f_1(K)$, $f_2(K)$, and $F_1(K)$. Then, with the flow properties known at some "initial" location, x_0 in the boundary layer, $K = K_0$ can be evaluated from Eq. (8). Next, dZ/dx can be calculated from Eq. (10) and utilized in an appropriate numerical algorithm to evaluate Z at a location Δx further downstream $(x_0 + \Delta x)$. With Z known at $(x_0 + \Delta x)$, $\Theta = \sqrt{\nu Z(x)}$ and, since u_e and du_e/dx are known at all x, K can be calculated at $(x_0 + \Delta x)$. The table provides the data to compute the functions and dZ/dx at the new location. The algorithm can be repeated until the end of the boundary-layer region of interest is reached or until the separation point ($\Lambda = -12$) is reached, at which time the calculations are normally terminated.

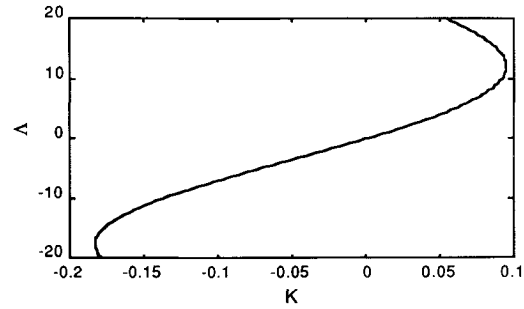

Fig. 1 Variation of the function $\Lambda(K)$.

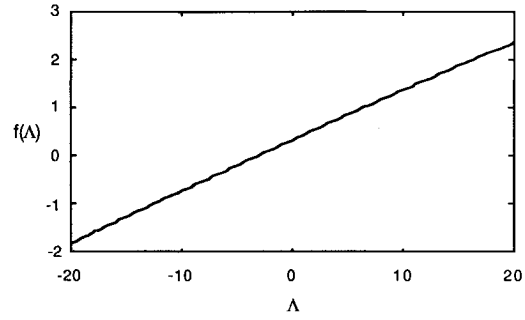

Fig. 2 Variation of $f(\Lambda)$.

This procedure is easily implemented for hand computations but, for computer applications, two approaches are possible. A table look up can be used in a table of functions. In order to avoid such time-consuming operations and to obtain greater accuracy, a root finder can be applied to Eq. (8) in order to find the Λ for given K. Then, Eqs. (9) and (10) can be used to evaluate the required functions and the boundary layer quantities.

The Correlation $\Lambda(K)$

The root finder is also a time-consuming operation that could be eliminated if Eq. (8) can be inverted to obtain $\Lambda(K)$ explicitly. $\Lambda(K)$ is plotted on Fig. 1 and suggests fitting $\Lambda(K)$ with a sine function. The roots of Eq. (8) in the form $K = (\Lambda - \Lambda_1)^2(\Lambda - \Lambda_2)^2(\Lambda - \Lambda_3)/9072^2$ are $\Lambda_1 = 28.1946$, $\Lambda_2 = -37.7945$, and $\Lambda_3 = 0$. The derivative can be written in the form $dK/d\Lambda = 5/9072^2\ (\Lambda - \Lambda_1)(\Lambda - \Lambda_2)(\Lambda - \Lambda_4)(\Lambda - \Lambda_5)$, where $\Lambda_4 = 12.0000$ and $K_{max} = 0.0948148$ at the maximum in K while $\Lambda_5 = -17.7600$ and $K_{min} = -0.182916$ at the minimum in K.

With these values, a function $f(\Lambda)$ was defined in Eq. (11) and is plotted in Fig. 2. The curve appears to be straight and a fit $f(\Lambda) = a + b\Lambda = 0.105564(2.88 + \Lambda)$ through the maximum and minimum points produces $f(0) = 0.304025$ when the exact value is 0.322796 with a 5.8% error. The fit in Eq. (12) where the coefficients are evaluated at the zero pressure-gradient point ($\Lambda = 0$), the separation point ($\Lambda = -12$), and the maximum point ($\Lambda = 12$) produces maximum relative error of 0.57% in the range $-20 \le \Lambda \le -12$, relative error of 0.17% in the range $-12 \le \Lambda \le 12$ and relative error increasing from 0.00014% at $\Lambda = 12$ to 1.88% at $\Lambda = 20$. As a final fit, a least-squares fit was obtained with the result in Eq. (13). This fit has a relative error in Λ decreasing from -0.12% at $\Lambda = -20$ to -0.34% at $\Lambda = -11.2$. Then, the relative error in Λ increases to 0.75% at $\Lambda = 11.6$ and decreases to -0.79% at $\Lambda = 20$. The rms error in the fit of $[a + b\Lambda + c\Lambda^2 - f(\Lambda)] = 0$ was 0.00395. Either of the fits in Eqs. (12) or (13) has a smaller relative error at large Λ. The quadratic for Λ from the combination of Eqs. (11-13) is easily solved and this Λ substituted into Eqs. (9) and (10) produces the quantities of interest for a given K.

$$f(\Lambda) = \sin^{-1}\left(\frac{K - K_0}{A}\right)$$

$$K_0 = \frac{1}{2}(K_{\max} - K_{\min}), \qquad A = \frac{1}{2}(K_{\max} - K_{\min}) \tag{11}$$

$$f(\Lambda) = a + b\Lambda + c\Lambda^2 =$$

$$0.32279550 + 0.10489340\Lambda - 0.000074444753\Lambda^2 \tag{12}$$

$$f(\Lambda) = a + b\Lambda + c\Lambda^2 =$$

$$0.32599640 + 0.10469083\Lambda - 0.00012134730\Lambda^2 \tag{13}$$

References

[1]White, F. M., *Viscous Fluid Flows,* McGraw-Hill, New York, 1974.

Euler Solutions for Delta Wings

Andrew B. Wardlaw Jr.* and Stephen F. Davis†
Naval Surface Warfare Center, Silver Spring, Maryland

Nomenclature

b = wing semispan
c = speed of sound
M = Mach number
M_c = Mach number of velocity component normal to ray from wing apex
M_s = Mach number of velocity component normal to upstream side of shock
p = pressure
S_s = (shock spanwise location)/b
s = entropy, $\ell n(p/p_\infty) - \gamma \ell n(\rho/\rho_\infty)$
α = angle of attack
Λ = wing sweep angle measured from normal to wing centerline
ρ = density
$\Sigma\Gamma_z$ = (z component of total crossflow plane circulation)/bc_∞

Subscript
∞ = freestream conditions

Introduction

Miller and Wood[1] have classified the experimentally observed flowfields occurring on delta wings into six different regimes as shown in Fig. 1. These regimes can be divided into three types of flow structures; those which are dominated by a strong leeside vortex, indicated by the dotted region in Fig. 1, those which feature a strong crossflow shock and the remaining regime which exhibits a separation bubble at the wing tip. Euler solutions for delta wings have been extensively studied and a review of this work is provided in Ref. 2. These solutions exhibit two types of structures; separated solutions which feature a large leeside vortex and attached solutions which are dominated by a leeside crossflow shock. Separated solutions are adequate engineering tools for predicting lift, surface pressure, and total pressure loss of the vortex dominated flows illustrated by the dotted regions in Fig. 1. However, the conditions under which computation yields a separated solution have not been systematically studied, and it is not clear that the domain of the computed separated solution coincides with the dotted area in Fig. 1. In fact, numerical experiments using wings of varying thickness, different meshes, varying levels of artificial viscosity and upwind as opposed to centrally differenced schemes show conflicting solution types for the same problem.[3-5] The purpose of this Note is to examine the conditions under which the separated solutions form, trace the evolution of the separated solution, and study the numerical factors which influence inviscid solution type.

Numerical Results

The flow over a delta wing is calculated by solving the steady Euler equations using a Godunov type scheme. The solution is obtained by marching along the delta wing centerline, starting from a uniform axial flow. This marching procedure is only valid for flowfields in which the axial component of velocity remains supersonic everywhere. On a conical body, the solution converges to a conically similar flow. Three variations of the Godunov method have been used. The complete Godunov scheme is a second-order Godunov scheme based on the complete Riemann problem. The approximate Godunov scheme is a second-order scheme which replaces the complete problem with an approximate one. The first-order Godunov scheme is based on the complete Riemann problem. Calculations have been completed using an elliptic, body-fitted coordinate system and a fitted bow shock. Details of the numerical scheme are provided in Ref. 6, and a more extensive description of the numerical results is provided in Ref. 7.

Domain of Attached and Detached Flow

The influence of Mach number and incidence on the occurrence of attached and separated flow is explored in Fig. 1 for zero-thickness wings. A boundary dividing the attached and separated solutions for the complete Godunov scheme is

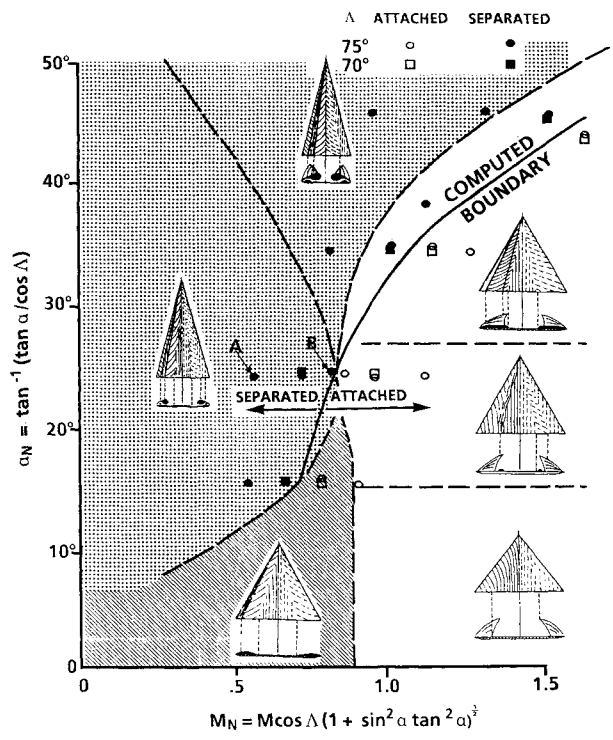

Fig. 1 Computed and measured flowfield type on a delta wing.

Received Dec. 4, 1989. This paper is declared a work of the U.S. Government and is not subject to copyright protection in the United States.

*Aerospace Engineer, Information and Mathematical Sciences Branch. Associate Fellow AIAA.
†Mathematician, Information and Mathematical Sciences Branch.